

High-order doubly localized waves in (2+1)-dimensional Maccari system

Xue-Wei Yan(严学威), Jin-Jin Mao(茆晋晋), and Min-Jie Dong(董敏杰)
Citation: Chin. Phys. B, 2026, 35 (**7**): 070201. DOI: 10.1088/1674-1056/ae0682
http://cpb.iphy.ac.cn; http://iopscience.iop.org/cpb

What follows is a list of articles you may be interested in

Multi-soliton solutions, breather-like and bound-state solitons for complex modified Korteweg-de Vries equation in optical fibers

Zhong-Zhou Lan(兰中周)
Chin. Phys. B, 2024, 33 (**6**): 060201. DOI: 10.1088/1674-1056/ad39d7

Interaction solutions and localized waves to the (2+1)-dimensional Hirota-Satsuma-Ito equation with variable coefficient

Xinying Yan(闫鑫颖), Jinzhou Liu(刘锦洲), and Xiangpeng Xin(辛祥鹏)
Chin. Phys. B, 2023, 32 (**7**): 070201. DOI: 10.1088/1674-1056/acb9f2

High-order rational solutions and resonance solutions for a (3+1)-dimensional Kudryashov-Sinelshchikov equation

Yun-Fei Yue(岳云飞), Jin Lin(林机), and Yong Chen(陈勇)
Chin. Phys. B, 2021, 30 (**1**): 010202. DOI: 10.1088/1674-1056/abb3f3

Lump and interaction solutions to the (3+1)-dimensional Burgers equation

Jian Liu(刘健), Jian-Wen Wu(吴剑文)
Chin. Phys. B, 2020, 29 (**3**): 030201. DOI: 10.1088/1674-1056/ab6964

Dynamics of three nonisospectral nonlinear Schrödinger equations

Abdselam Silem, Cheng Zhang(张成), Da-Jun Zhang(张大军)
Chin. Phys. B, 2019, 28 (**2**): 020202. DOI: 10.1088/1674-1056/28/2/020202

High-order doubly localized waves in (2+1)-dimensional Maccari system

Xue-Wei Yan(严学威)[1,†], Jin-Jin Mao(茆晋晋)[1], and Min-Jie Dong(董敏杰)[2]

[1] *School of Science, Nanjing University of Posts and Telecommunications, Nanjing* 210023, *China*
[2] *School of Physical and Mathematical Sciences, Nanjing Tech University, Nanjing* 211816, *China*

(Received 28 August 2025; revised manuscript received 10 September 2025; accepted manuscript online 15 September 2025)

In this work, we explore the doubly localized wave solutions for the (2+1)-dimensional Maccari system using Hirota's bilinear method and Kadomtsev–Petviashvili (KP) hierarchy reduction method. These solutions illustrate the temporal evolution of a line rogue wave and a lump in the background of a breather or homoclinic orbit. The line rogue wave in these solutions is characterized by two endpoints, and is thus referred to as a line-segment rogue wave. The lump is also a doubly localized wave known as a rogue lump, which is also localized in both time and two spatial dimensions. These waves emerge from the breather waves or homoclinic orbits and remain unchanged for a short period of time, eventually merging into other breather waves or homoclinic orbits. Notably, these rogue lumps appear and vanish alongside the homoclinic orbits and play a significant role in understanding extreme events in physical scenarios.

Keywords: Maccari system, bilinear form, Schur polynomial, doubly localized wave, homoclinic orbit

PACS: 02.30.IK, 03.75.Nt, 02.30.Hq

DOI: 10.1088/1674-1056/ae0682 **CSTR:** 32038.14.CPB.ae0682

1. Introduction

The study on the collision behavior of localized waves with other waves in two- and high-dimensional nonlinear integrable systems is of significant importance in the field of nonlinear science.[1] These nonlinear integrable systems consist of several important solitons, such as lump, rogue wave, line soliton, breather, and others. Lump as a kind of localized wave remains a local feature in two-dimensional (2D) space and has an important significance in the study of the formation and evolution of extreme wave events in various fields, including nonlinear optics,[2] plasma,[3] Bose–Einstein condensate,[4] and shallow water surface.[5] Lump solitons maintain their shapes and amplitudes unchanged during the process of temporal evolution. However, they undergo changes through nonelastic interactions with other solitons. The rogue wave phenomenon was initially discovered by Draper[6] and is characterized by "appear from nowhere and disappear without a trace".[7] A rogue wave, also known as a monster wave or killer wave, is characterized by having a wave height more than twice that of the surrounding waves. This phenomenon is not only observed in the ocean but also in other fields, such as space plasma,[8,9] optics,[10] Bose–Einstein condensate,[11] atmosphere,[12] and finance.[13] A rogue wave typically manifests as a nonlinear wave in high-dimensional systems, demonstrating infinite length and temporal localization but not spatial localization.[14,15] Breather, also known as periodic soliton, can be classified according to its locality and periodicity in time and space. These classifications include the Akhmediev breather,[16] Kuznetsov–Ma soliton,[17,18] Tajiri–Watanabe breather,[19] and line breather (also referred to as homoclinic orbit). Interaction of these breathers leads to breather molecules,[20,21] and super breathers.[22,23] To describe the phenomena of these nonlinear waves in various fields, important methods have been proposed, including the Darboux transformation,[24–28] inverse scattering method,[29–31] Hirota's bilinear method,[32] KP hierarchy reduction method,[33–37] *etc*. Regarding these aspects, our team has reported some significant results.[38–43]

It is worth noting that lump, line rogue wave and homoclinic orbit only arise in high-dimensional nonlinear systems.[44–47] These solitons and their mixtures can be mathematically described by the (semi-)rational solutions. The resonant collisions between these waves generate some intriguing waveforms, which were initially investigated by Miles.[48,59] Recently, the emission and absorption of lumps in soliton backgrounds have garnered significant attention from researchers. The time evolution processes involving lumps emerging from breathers and subsequently merging into other breathers are referred to as complete resonant collisions. These collisions result in lumps that are doubly localized in both time and space, commonly known as rogue lumps.[50] Chen *et al*. have studied the rogue wave of the massive Thirring model and nonlocal nonlinear Schrödinger equation by virtue of the KP reduction and physics-informed neural network method, respectively.[51,52] Dai *et al*. have researched the collapse of soliton-like bubble by cavitation leading to launch-

†Corresponding author. E-mail: xwyan16@163.com

© 2026 Chinese Physical Society and IOP Publishing Ltd. All rights, including for text and data mining, AI training, and similar technologies, are reserved.

ing of microbots.[53] However, our works focus on the construction of the double localized wave consisting of the lump and multi-breather waves, which show a complete resonant collision process between the lump and breathers. Furthermore, these lumps likely emerge from the background of homoclinic orbits and decay alongside the latter towards a constant state during time evolution.[54] Recently, Ma[55,56] introduced a new method to get the lump solutions or lump-type solutions of the equation by using Hirota's bilinear method.

In this paper, we concentrate on the high-order doubly localized waves for the (2+1)-dimensional Maccari system[57]

$$\begin{cases} \mathrm{i}u_t + L_1 u + uv = 0, L_2 v - 2L_1|u|^2 = 0, \\ L_1 = \dfrac{1}{4}(1 - s\lambda^2)\partial_{xx} + s\lambda\,\partial_{xy} - s\partial_{yy}, \\ L_2 = -\dfrac{1}{4}(1 + s\lambda^2)\partial_{xx} + s\lambda\,\partial_{xy} - s\partial_{yy}, \end{cases} \tag{1}$$

where u, v are the complex functions of time t and spatial variables x, y, while s and λ denote arbitrary real constants. Maccari initially proposed this equation by utilizing a reduction method that relied on spatial–temporal rescaling. This equation can be applied to describe the nonlinear phenomena in 2D systems, such as water waves, nonlinear optics, photonics, and matter waves in Bose–Einstein condensates. Recently, Maccari has demonstrated that this equation serves as a generic model for describing rogue waves in various physical settings.[58] Regarding this model, Rao *et al.* constructed semi-rational solutions to analyze the complete resonant collision between lumps, breathers, and multi-line solitons.[59] Fusion and fission collisions between lumps and multi-breathers have been reported in Ref. [60]. Furthermore, the interactions of line solitons, lumps and line rogue waves for the nonlocal Maccari system have been investigated using Hirota's bilinear method.[47] Bright–dark mixed soliton solutions have been reported in Ref. [61]. Ma derived the rogue wave solution of the coupled Maccari system using the truncated Painlevé approach, and Meng studied a 2D multi-component Maccari system and obtained nondegenerate soliton solutions.[62,63] To the best of our knowledge, the consideration of the rogue lump and line-segment rogue wave in a breather or a homoclinic orbit background is lacking. Therefore, the following three problems arise:

(i) How do the doubly localized waves move between breathers, and what variations do the amplitudes of these lumps exhibit?

(ii) What occurs when the doubly localized waves emerge and vanish from the homoclinic orbit during the time evolution?

(iii) How do the shapes and intensities of high-order doubly localized waves transform in the presence of a breather or homoclinic orbit background?

To solve these problems, we construct the double localized wave solutions of the Maccari system using the KP reduction method. Additionally, we also analyze the time evolution behaviors of lumps in the backgrounds of multi-breathers or homoclinic orbits using the parameter restriction and maximum amplitude function analysis method. Our objective is to utilize the KP reduction method to construct the semi-rational solutions in the form of a Schur polynomial. These solutions are intended to describe the complete resonant collision between localized waves and breather waves. We will analyze the behavior of first- and high-order doubly localized waves as they propagate in the background of breathers or homoclinic orbits.

The structure of the paper is arranged as follows: In Section 2, we derive the semi-rational solutions of the (2+1)-dimensional Maccari system by combining Hirota's bilinear method and the KP hierarchy reduction method. In Section 3, we provide a detailed analysis of the simplest doubly localized wave solution, which involves two doubly localized waves. In Section 4, we theoretically and graphically discuss the presence of high-order doubly localized waves in a three-breather or homoclinic orbit background. Finally, in the last section, we discuss these results.

2. Bilinearization and doubly localized wave solutions

In this section, we construct the semi-rational solutions by employing the KP hierarchy reduction method. To accomplish this, we first derive the bilinear form in the following lemma.

Lemma 1 (2+1)-dimensional Maccari system (1) converts to the bilinear form

$$\left[\mathrm{i}D_t + \frac{1}{4}(1 - s\lambda^2)D_x^2 + s\lambda D_x D_y - sD_y^2\right] g\cdot f = 0, \tag{2}$$

$$\left[2 - \frac{1}{4}(1 + s\lambda^2)D_x^2 + s\lambda D_x D_y - sD_y^2\right] f\cdot f = 2|g|^2, \tag{3}$$

via the dependent variable transformations

$$u(x,y,t) = \frac{g(x,y,t)}{f(x,y,t)},$$
$$v(x,y,t) = 2L_1 \ln f(x,y,t),$$

where $f(x,y,t)$ represents a real function and $g(x,y,t)$ denotes a complex function to be determined later. L_1 is the differential operator given by system (1). D represents Hirota's bilinear operator.[32]

Theorem 1 (2+1)-dimensional Maccari system admits $(K+1)$th-order doubly localized wave solutions

$$u(x,y,t) = \frac{g(x,y,t)}{f(x,y,t)}, \quad v(x,y,t) = 2L_1 \ln f(x,y,t), \tag{4}$$

where $g = \tau_1, f = \tau_0$ are provided by a tau-function

$$\tau_n = \det_{1\le i,j\le N}\left(m_{ij}^{(n)}\right),$$

where the element $m_{ij}^{(n)}$ is given by

$$\begin{aligned}
m_{ij}^{(n)} &= \sum_{k=1}^{2}\sum_{l=1}^{2}\left(-\frac{p_k}{p_l^*}\right)^n \mathrm{e}^{\xi_k+\xi_l^*+\xi_{ik}^{(0)}+\xi_{jl}^{(0)*}} \\
&\quad\times \sum_{\sigma=0}^{2K+2-i-j}\frac{(-1)^\sigma}{\left(p_k+p_l^*\right)^{\sigma+1}}\partial_{x_1}^{\sigma}P_{ik}(n)P_{jl}^*(-n), \\
P_{ik}(n) &= \sum_{\alpha=0}^{K+1-i} a_{ik}^{[\alpha]} S_{K+1-\alpha}\left(\boldsymbol{x}_k(n)\right), \\
\boldsymbol{x}_k(n) &= \left(x_{1k}+n, x_{2k}, \ldots, x_{rk}, \ldots\right), \\
x_{rk} &= \frac{(-2)^r}{r!p_k^2}x_{-2}+\frac{(-1)^r}{r!p_k}x_{-1}+\frac{1}{r!}p_k x_1+\frac{2^r}{r!}p_k^2 x_2, \\
\xi_k &= \sum_{\nu=-2,-1,1,2} p_k^\nu x_\nu,
\end{aligned}$$

where x_ν, $(\nu=-2,-1,1,2)$ are given by Eq. (13).

Proof Based on the Sato theory[14,15] and Ref. [64] we give the bilinear KP hierarchy

$$(D_{x_1}^2-D_{x_2})\tau_{n+1}\cdot\tau_n=0, (D_{x_{-1}}^2+D_{x_{-2}})\tau_{n+1}\cdot\tau_n=0, \quad (5)$$

$$(D_{x_1}D_{x_{-1}}-2)\tau_n\cdot\tau_n=-2\tau_{n+1}\cdot\tau_{n-1}, \quad (6)$$

which has the Gram-type solution

$$\tau_n=\det_{1\le i,j\le N}\left(m_{ij}^{(n)}\right).$$

$m_{ij}^{(n)}$ denotes the complex functions and satisfies the differential and difference equations

$$\begin{aligned}
&m_{ij}^{(n+1)}=m_{ij}^{(n)}+\psi_i^{(n)}\phi_j^{(n+1)}, \\
&\partial_{x_{-1}}m_{ij}^{(n)}=-\psi_i^{(n-1)}\phi_j^{(n+1)}, \\
&\partial_{x_{-2}}m_{ij}^{(n)}=-\psi_i^{(n-2)}\phi_j^{(n+1)}-\psi_i^{(n-1)}\phi_j^{(n)}, \\
&\partial_{x_1}m_{ij}^{(n)}=\psi_i^{(n)}\phi_j^{(n)}, \\
&\partial_{x_2}m_{ij}^{(n)}=\psi_i^{(n+1)}\phi_j^{(n)}+\psi_i^{(n)}\phi_j^{(n-1)}, \\
&\partial_{x_\nu}\psi_i^{(n)}=\psi_i^{(n+\nu)}, \quad \partial_{x_\nu}\phi_j^{(n)}=-\phi_j^{(n-\nu)},
\end{aligned}$$

where $\nu=-2,-1,1,2$ and $\psi_i^{(n)},\phi_j^{(n)}$ are the complex functions of the variables x_ν. In order to construct the doubly localized wave solutions of system (1), we suppose three functions

$$\begin{aligned}
&m_{ij}^{(n)}=\int_{-\infty}^{x_1}\psi_i^{(n)}\phi_j^{(n)}d_{x_1}, \quad \psi_i^{(n)}=\sum_{k=1}^{2}A_{ik}p_k^n\mathrm{e}^{\xi_{ik}}, \\
&\phi_j^{(n)}=\sum_{l=1}^{2}B_{jl}\left(-q_l\right)^{-n}\mathrm{e}^{\eta_{jl}},
\end{aligned}$$

where the differential operators A_{ik},B_{jl} and the complex line functions ξ_{ik},η_{jl} are defined as

$$\begin{aligned}
A_{ik}\left(p_k\right)&=\sum_{\alpha=0}^{K+1}\frac{a_{ik}^{[\alpha]}}{(K+1-\alpha)!}\left(p_k\partial_{p_k}\right)^{K+1-\alpha}, \\
B_{jl}\left(q_l\right)&=\sum_{\beta=0}^{K+1}\frac{b_{jl}^{[\beta]}}{(K+1-\beta)!}\left(q_l\partial_{q_l}\right)^{K+1-\beta}, \\
\xi_{ik}&=\xi_k+\xi_{ik}^{(0)}, \quad \xi_k=\sum_{\nu=-2,-1,1,2}p_k^\nu x_\nu, \\
\eta_{jl}&=\eta_l+\eta_{jl}^{(0)}, \quad \eta_l=\sum_{\nu=-2,-1,1,2}q_l^\nu x_\nu.
\end{aligned}$$

Here p_k, q_l, $\xi_{ik}^{(0)}$, $\eta_{jl}^{(0)}$ are the complex constants. In addition, we can obtain

$$\sum_{\alpha=0}^{K+1}\frac{a_{ik}^{[\alpha]}}{(K+1-\alpha)!}\left(p_k\partial_{p_k}\right)^{K+1-\alpha}p_k^n\mathrm{e}^{\xi_{ik}}=P_{ik}(n)p_k^n\mathrm{e}^{\xi_{ik}}, \quad (7)$$

$$\begin{aligned}
&\sum_{\beta=0}^{K+1}\frac{b_{jl}^{[\beta]}}{(K+1-\beta)!}\left(q_l\partial_{q_l}\right)^{K+1-\beta}\left(-q_l\right)^{-n}\mathrm{e}^{\eta_{jl}} \\
&=Q_{jl}(n)\left(-q_l\right)^{-n}\mathrm{e}^{\eta_{jl}}, \quad (8)
\end{aligned}$$

where $P_{ik}(n)$, $Q_{jl}(n)$ are the functions of x_ν. Integrating by parts yields

$$\begin{aligned}
m_{ij}^{(n)} &= c_{ij}+\sum_{k=1}^{2}\sum_{l=1}^{2}\left(-\frac{p_k}{q_l}\right)^n\mathrm{e}^{\xi_{ik}+\eta_{jl}} \\
&\quad\times\sum_{\sigma=0}^{2K+2}\frac{(-1)^\sigma}{\left(p_k+q_l\right)^{\sigma+1}}\partial_{x_1}^{\sigma}P_{ik}(n)Q_{jl}(n).
\end{aligned}$$

Without loss of generality, we can take the integration constant $c_{ij}=0$. If we let

$$p_k=q_k^*, \quad \xi_{ik}^{(0)}=\eta_{ik}^{(0)*}, \quad a_{ik}^{[\alpha]}=b_{ik}^{[\alpha]*},$$

and x_{-1},x_1 be real, one yields

$$\xi_{ik}=\eta_{ik}^*, \quad \xi_k'=\left(\eta_k'\right)^*, \quad P_{ik}(n)=Q_{ik}^*(-n), \quad (9)$$

$$m_{ij}^{(n)}=\left(m_{ji}^{(-n)}\right)^*, \quad \tau_n=\tau_{-n}^*. \quad (10)$$

Next, in order to calculate the function $P_{ik}(n)$, we give

$$\left(p_k\partial_{p_k}\right)^r p_k^n\mathrm{e}^{\xi_{ik}}=S_r p_k^n\mathrm{e}^{\xi_{ik}},$$

where $S_r=S_r\left(p_k\right)$ is a Schur polynomial. We further obtain a recurrence relation

$$\begin{aligned}
&\left(p_k\partial_{p_k}\right)^{r+1}p_k^n\mathrm{e}^{\xi_{ik}} \\
&=\left(p_k\partial_{p_k}\right)\left[\left(p_k\partial_{p_k}\right)^r p_k^n\mathrm{e}^{\xi_{ik}}\right]=\left(p_k\partial_{p_k}\right)\left[S_r(p_k)p_k^n\mathrm{e}^{\xi_{ik}}\right] \\
&=\left[p_k\partial_{p_k}S_r\left(p_k\right)+\xi_k'S_r\left(p_k\right)\right]p_k^n\mathrm{e}^{\xi_{ik}}=S_{r+1}(p_k)p_k^n\mathrm{e}^{\xi_{ik}},
\end{aligned}$$

where the derivative function ξ_k' is given as

$$\xi_k'=-\frac{2}{p_k^2}x_{-2}-\frac{1}{p_k}x_{-1}+p_k x_1+2p_k^2x_2.$$

One easily obtains

$$\begin{aligned}
&p_k^{-n}\mathrm{e}^{-\xi_{ik}}\mathrm{e}^{\varepsilon p_k\partial_{p_k}}p_k^n\mathrm{e}^{\xi_{ik}} \\
&=\exp\left[n\varepsilon+\xi_{ik}\left(\mathrm{e}^{\varepsilon}p_k\right)-\xi_{ik}\left(p_k\right)\right] \\
&=\exp\left(\sum_{r=1}^{\infty}\varepsilon^r x_{rk}\right)=\sum_{r=0}^{\infty}\varepsilon^r S_r\left(\boldsymbol{x}_k(n)\right), \quad (11)
\end{aligned}$$

with

$$\boldsymbol{x}_k(n) = (x_{1k}+n, x_{2k}, \ldots, x_{rk}, \ldots),$$
$$x_{rk} = \frac{(-2)^r}{r!p_k^2}x_{-2} + \frac{(-1)^r}{r!p_k}x_{-1} + \frac{1}{r!}p_k x_1 + \frac{2^r}{r!}p_k^2 x_2.$$

Comparing the coefficient of ε^r in Eq. (11), we obtain

$$p_k^{-n}\mathrm{e}^{-\xi_{ik}}\frac{\left(p_k\partial_{p_k}\right)^r}{r!}p_k^n\mathrm{e}^{\xi_{ik}} = S_r\left(\boldsymbol{x}_k(n)\right). \tag{12}$$

According to Eqs. (7)–(12), it is not hard to find

$$P_{ik}(n) = \sum_{\alpha=0}^{K+1} a_{ik}^{[\alpha]} S_{K+1-\alpha}\left(\boldsymbol{x}_k(n)\right).$$

Supposing $g=\tau_1$, $f=\tau_0$, under the complex symmetry conditions (9)–(10), and using variable transformations

$$x_{-2} = x_2^* = -\frac{\mathrm{i}}{2}t, \quad x_{-1} = x + \left(\lambda - \frac{\lambda\sqrt{-s}-1}{2\sqrt{-s}}\right)y,$$

$$x_1 = x + \frac{\lambda\sqrt{-s}-1}{2\sqrt{-s}}y, \tag{13}$$

the solutions (4) of the bilinear KP hierarchy (5)–(6) also satisfy the bilinear equations (2)–(3). Without loss of generality, we can set $a_{ik}^{[0]}=1, a_{ik}^{[\alpha]}=0, \alpha\neq 0, s=-\frac{1}{4}, \lambda=1$ in the next study. Furthermore, it is not difficult to find that p_1, p_2 are not pure imaginary constants.

3. Doubly localized waves in the two-breather/homoclinic orbit background

In this section, taking $K=1$ in Theorem 1, we derive the second-order doubly localized wave solution as follows:

$$\begin{aligned}
\tau_n =\ & \left(T_1^{[1,1]}T_4^{[1,1]} - T_2^{[1,1]}T_3^{[1,1]}\right)\mathrm{e}^{2\xi_1^{(0)}+2\xi_2^{(0)}}\mathrm{e}^{2\zeta+2\zeta^*} + T_1^{[2,2]}T_4^{[2,2]} - T_2^{[2,2]}T_3^{[2,2]} \\
&+\left[\left(T_1^{[1,1]}T_4^{[1,2]} - T_2^{[1,2]}T_3^{[1,1]}\right)\mathrm{e}^{\xi_1^{(0)}} + \left(T_1^{[1,2]}T_4^{[1,1]} - T_2^{[1,1]}T_3^{[1,2]}\right)\mathrm{e}^{\xi_2^{(0)}}\right]\mathrm{e}^{\xi_1^{(0)}+\xi_2^{(0)}}\mathrm{e}^{2\zeta+\zeta^*} \\
&+\left[\left(T_1^{[1,1]}T_4^{[2,1]} - T_2^{[1,1]}T_3^{[2,1]}\right)\mathrm{e}^{\xi_1^{(0)}} + \left(T_1^{[2,1]}T_4^{[1,1]} - T_2^{[2,1]}T_3^{[1,1]}\right)\mathrm{e}^{\xi_2^{(0)}}\right]\mathrm{e}^{\xi_1^{(0)}+\xi_2^{(0)}}\mathrm{e}^{\zeta+2\zeta^*} \\
&+\left(T_1^{[1,2]}T_4^{[1,2]} - T_2^{[1,2]}T_3^{[1,2]}\right)\mathrm{e}^{\xi_1^{(0)}+\xi_2^{(0)}}\mathrm{e}^{2\zeta} + \left(T_1^{[2,1]}T_4^{[2,1]} - T_2^{[2,1]}T_3^{[2,1]}\right)\mathrm{e}^{\xi_1^{(0)}+\xi_2^{(0)}}\mathrm{e}^{2\zeta^*} \\
&+\left[\left(T_1^{[1,1]}T_4^{[2,2]} - T_2^{[1,2]}T_3^{[2,1]}\right)\mathrm{e}^{2\xi_1^{(0)}} + \left(T_1^{[2,2]}T_4^{[1,1]} - T_2^{[2,1]}T_3^{[1,2]}\right)\mathrm{e}^{2\xi_2^{(0)}}\right. \\
&\left.+\left(T_1^{[2,1]}T_4^{[1,2]} - T_2^{[2,2]}T_3^{[1,1]} + T_1^{[1,2]}T_4^{[2,1]} - T_2^{[1,1]}T_3^{[2,2]}\right)\mathrm{e}^{\xi_1^{(0)}+\xi_2^{(0)}}\right]\mathrm{e}^{\zeta+\zeta^*} \\
&+\left[\left(T_1^{[1,2]}T_4^{[2,2]} - T_2^{[1,2]}T_3^{[2,2]}\right)\mathrm{e}^{\xi_1^{(0)}} + \left(T_1^{[2,2]}T_4^{[1,2]} - T_2^{[2,2]}T_3^{[1,2]}\right)\mathrm{e}^{\xi_2^{(0)}}\right]\mathrm{e}^{\zeta} \\
&+\left[\left(T_1^{[2,1]}T_4^{[2,2]} - T_2^{[2,2]}T_3^{[2,1]}\right)\mathrm{e}^{\xi_1^{(0)}} + \left(T_1^{[2,2]}T_4^{[2,1]} - T_2^{[2,1]}T_3^{[2,2]}\right)\mathrm{e}^{\xi_2^{(0)}}\right]\mathrm{e}^{\zeta^*},
\end{aligned} \tag{14}$$

where

$$\begin{aligned}
T_1^{[k,l]} &= \frac{1}{p_k+p_l^*}\left(-\frac{p_k}{p_l^*}\right)^n\left[\left(x_{1k}+n-\frac{p_k}{p_k+p_l^*}\right)\right. \\
&\quad\left.\times\left(x_{1l}^*-n-\frac{p_l^*}{p_k+p_l^*}\right)+\frac{p_kp_l^*}{(p_k+p_l^*)^2}\right], \\
T_2^{[k,l]} &= \frac{1}{p_k+p_l^*}\left(-\frac{p_k}{p_l^*}\right)^n\left(x_{1k}+n-\frac{p_k}{p_k+p_l^*}\right), \\
T_4^{[k,l]} &= \frac{1}{p_k+p_l^*}\left(-\frac{p_k}{p_l^*}\right)^n, \\
T_3^{[k,l]} &= \frac{1}{p_k+p_l^*}\left(-\frac{p_k}{p_l^*}\right)^n\left(x_{1l}^*-n-\frac{p_l^*}{p_k+p_l^*}\right), \\
\zeta &= \xi_1-\xi_2, \xi_i^{(0)} = \xi_{i1}^{(0)}-\xi_{i2}^{(0)}.
\end{aligned}$$

This solution is regarded as the simplest doubly localized wave solution comprising two rational waves and two breathers. In this complete resonant collision process, only one of two rational waves can appear for a short time. This is because the resonant collision leads to the assimilation of another rational wave at the initial state of interaction. This doubly localized feature is formed by the resonant collision between the rational waves and two breathers. It is also similar to the interaction behaviors between the rational wave and two line solitons, but the distinction is that only one rational wave exists in the line soliton background. The states of these two rational waves are determined by the phase difference. When one sets $\xi_1^{(0)}>0$, the rational wave determined by p_1 appears and moves along the trajectory $x_{11}\approx 0$ between two breathers, meanwhile the other rational wave determined by p_2 disappears. When one sets $\xi_1^{(0)}<0$, the rational wave determined by p_2 appears and moves along the trajectory $x_{12}\approx 0$ between two breathers. When one sets $\xi_1^{(0)}\approx 0$, there are only two breathers in the constant background, and they become compact near $t=0$. It is worth mentioning that the two rational waves can be identified by the solution $u_{\mathrm{rational}} = T_{11}(1)/T_{11}(0)$, where $T_{11}(n)$ is the coefficient of $\mathrm{e}^{\zeta+\zeta^*}$ in Eq. (14). In addition, these rational waves can be divided into two cases: (i) line rogue wave ($p_{kl}=0$); (ii) lump ($p_{kl}\neq 0$), in which the line rogue wave in the doubly localized wave solution, is also referred as a line-

segment rogue wave with a finite wavelength. On the other hand, a rogue lump is a localized phenomenon that occurs in both time and two-dimensional space. These two types of waves are doubly localized wave in 2D physical setting.

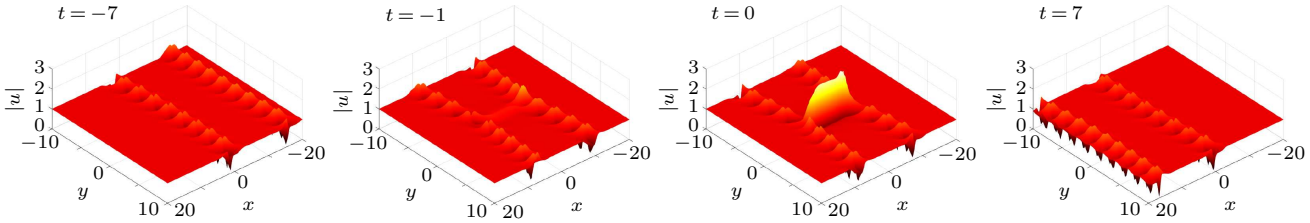


Fig. 1. The time evolution of line-segment rogue wave in the background of two-breather via parameters: $p_1 = 1$, $p_2 = \frac{1}{5} - \frac{1}{2}\mathrm{i}$, $\xi_{11}^{(0)} = -\xi_{21}^{(0)} = 2\pi$.

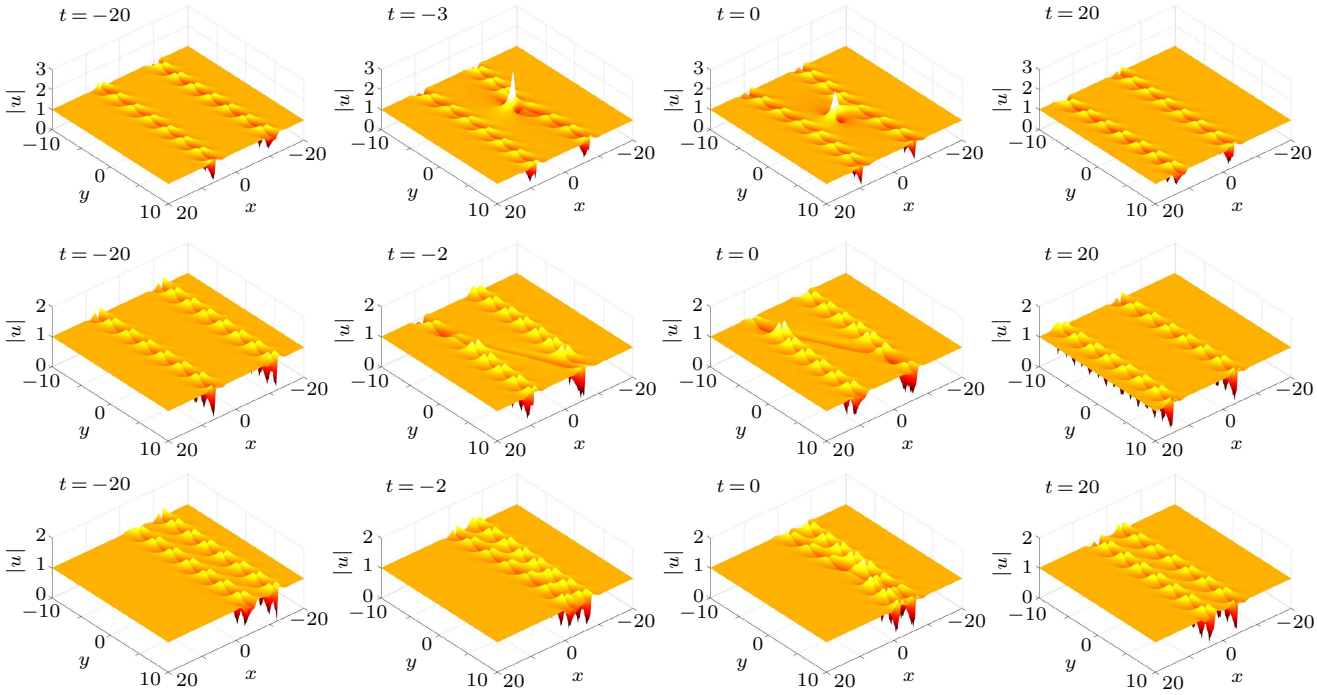


Fig. 2. The time evolution of a rogue lump in the background of two-breather via parameters: $p_1 = 1 - \frac{1}{2}\mathrm{i}$, $p_2 = \frac{7}{50} - \frac{1}{2}\mathrm{i}$, the first line: $\xi_{11}^{(0)} = -\xi_{21}^{(0)} = 2\pi$, the second line: $\xi_{11}^{(0)} = -\xi_{21}^{(0)} = -2\pi$, and the third line: $\xi_{11}^{(0)} = \xi_{21}^{(0)} = 2\pi$.

Next, we show the interaction between the line-segment rogue wave and two breathers. As depicted in Fig. 1, we display the four states of a line-segment rogue wave with x-direction during the complete resonant collision process at times $t = -7, -1, 0, 7$. The line-segment rogue wave appears from two breathers with unchanged period at time $t = -1$ and attains the highest peak at $t = 0$. At the same time, two breathers move along the positive x-direction. Finally, the line wave is absorbed into the background due to the resonant collision of these waves. At the stages of input and output, there is no line-segment rogue wave in the breather background. Without loss of generality, if we let $p_1 = k - \frac{1}{2}\mathrm{i}$ in the first-order rational solution, one obtains three critical points $(x_i, y_i), (i = 1, 2, 3)$ which are identified by the conditions $\Delta_x = 0, \Delta_y = 0$. The maximum point satisfies the second-order derivative conditions $\Delta > 0, \tilde{\Delta} < 0$. The minimum point satisfies the second-order derivative conditions $\Delta > 0, \tilde{\Delta} > 0$, where

$$\Delta_x = \frac{\partial|u|}{\partial_x}, \quad \Delta_y = \frac{\partial|u|}{\partial_y},$$
$$\Delta = \frac{\partial^2|u|\partial^2|u|}{\partial_{x^2}\partial_{y^2}} - \frac{\partial^2|u|}{\partial_x\partial_y}, \quad \tilde{\Delta} = \frac{\partial^2|u|}{\partial_{x^2}}.$$

By calculating these conditions, we obtain three types of lumps that correspond to the intervals of k as follows: Bright lump contains a maximum point (x_1, y_1) and two minimum points $(x_{3\pm}, y_{3\pm})$, when $k \in (-\infty, -\frac{\sqrt{3}}{2}] \cup [\frac{\sqrt{3}}{2}, +\infty)$; Four-petal lump contains two maximum points $(x_{2\pm}, y_{2\pm})$ and two minimum points $(x_{3\pm}, y_{3\pm})$, when $k \in (-\frac{\sqrt{3}}{2}, -\frac{1}{4}\sqrt{2\sqrt{17}-2}) \cup (\frac{1}{4}\sqrt{2\sqrt{17}-2}, \frac{\sqrt{3}}{2})$; Dark lump contains two maximum points $(x_{2\pm}, y_{2\pm})$ and a minimum point (x_1, y_1), when $k \in [-\frac{1}{4}\sqrt{2\sqrt{17}-2}, \frac{1}{4}\sqrt{2\sqrt{17}-2}]$. Now, assuming the parameters $p_1 = 1 - \frac{1}{2}\mathrm{i}, p_2 = \frac{7}{50} - \frac{1}{2}\mathrm{i}$, the complete resonant solution comprises a bright rogue lump and a dark rogue lump together with two breathers. According to the results presented above, the phase parameters $\xi_{11}^{(0)}, \xi_{21}^{(0)}$ can be cho-

sen as three cases, which correspond to the different interaction phenomena. If we choose $\xi_{11}^{(0)} = 2\pi, \xi_{21}^{(0)} = -2\pi$, as shown in Fig. 2, a bright rogue lump appears from the right breather and moves along the trajectory $(\frac{393t}{320}, \frac{57t}{160})$; meanwhile, the dark rogue lump disappears from the breather background since it is absorbed in the initial state. By calculating the bright rogue lump, we can obtain a maximum point $(\frac{393t}{320} + \frac{1051}{6536}, \frac{57t}{160} - \frac{1051}{9804})$ and two minimum points $(\frac{393t}{320} + \frac{1051}{6536} - \frac{7\sqrt{11}}{128}, \frac{57t}{160} - \frac{1051}{9804} + \frac{9\sqrt{11}}{64})$. After that, the bright rogue lump disappears into the left breather at about $t = 10$. As shown in Fig. 3(a), the overlapping part of the blue solid line (denoting the maximum amplitude of the rogue lump) and the yellow dashed line (representing the minimum amplitude of the rogue lump) indicates that there is no rogue lump between two breathers. In the non-overlapping part, the vibration continuously occurring in the amplitude curve shows that this rogue lump changes its amplitude for a short time. Thus, we do not present its extreme amplitude. Furthermore, if we let $\xi_{11}^{(0)} < \xi_{21}^{(0)}$, *i.e.*, $\xi_{11}^{(0)} = -2\pi, \xi_{21}^{(0)} = 2\pi$, there is only the dark rogue lump in the same breather background but the bright rogue lump disappears. Similarly, we can obtain a maximum point $(\frac{3317281503}{2106250000}t + \frac{96275}{22876}, -\frac{2956813497}{1053125000}t - \frac{96275}{34314})$ and a minimum point $(\frac{3317281503}{2106250000}t + \frac{96275}{22876} - \frac{4087\sqrt{1826}}{70000}, -\frac{2956813497}{1053125000}t - \frac{96275}{34314} + \frac{913\sqrt{1826}}{35000})$. Thus, one can obtain the dark rogue lump with velocity $(\frac{3317281503}{2106250000}t, -\frac{2956813497}{1053125000}t)$, which moves along the line $1971208998x + 1105760501y = 0$ and merges into the other breather. The main part of the dark lump is located below the plane (also shown in Fig. 3). When one chooses $\xi_{11}^{(0)} = \xi_{21}^{(0)} = 2\pi$, as observed in the third line in Fig. 2, only two breathers move along the x-direction and show the processes of concentration and separation.

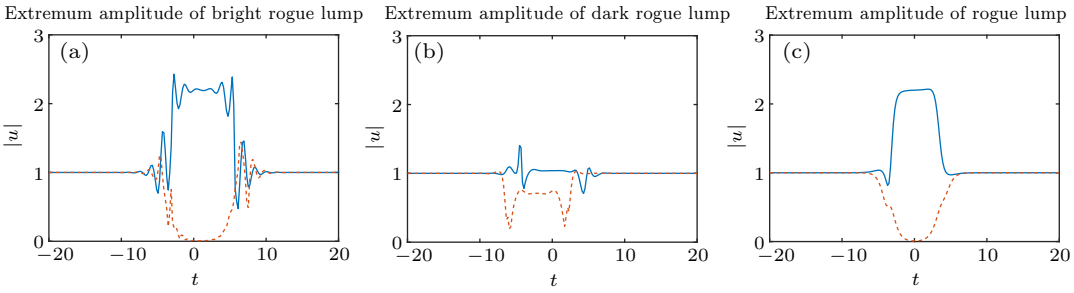


Fig. 3. The extremum amplitudes of rogue lump in the backgrounds of two-breather or two homoclinic orbits correspond to Figs. 2 and 5. Blue solid lines represent the maximum amplitude of the rogue lumps, while yellow dashed lines represent the minimum amplitude of the rogue lumps.

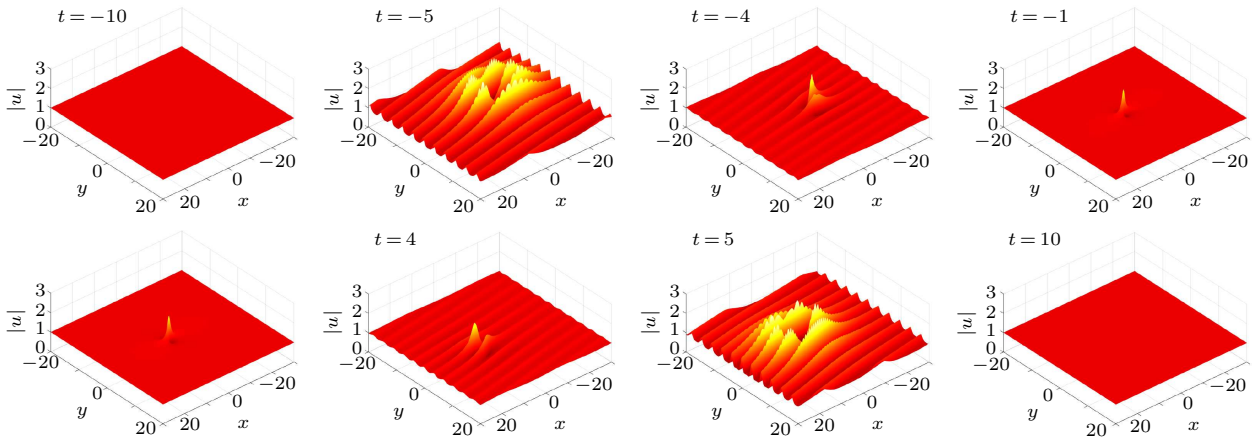


Fig. 4. The time evolution of a rogue lump in the background of two homoclinic orbits via parameters: $p_1 = p_2^* = 1 - \frac{1}{2}\mathrm{i}$, $\xi_{11}^{(0)} = -\xi_{21}^{(0)} = 2\pi$.

An interesting phenomenon is that breather waves transform to line breathers, also called homoclinic orbits, in the plane if one satisfies the parameter relation $p_1 = p_2^*$. This kind of line breather originates from the oscillation of a plane wave and decays to the constant background after a period of existence. Based on this character, we consider the doubly localized wave solution comprising two homoclinic orbits and two lumps by choosing $p_1 = 1 - \frac{1}{2}\mathrm{i}, \xi_{11}^{(0)} = -\xi_{21}^{(0)} = 2\pi$. In Fig. 4, a bright lump together with two homoclinic orbits appears and disappears in the constant background. As time t evolves, a wave packet appears from the homoclinic orbit background at time $t = -5$. The energy of other line waves transfers to the raised position, which excites a peak (see Fig. 4 at time $t = -4$). Then this lump remains unchanged over a short period of time from the disappearance of an old homoclinic orbit to the generation of a new homoclinic orbit. Through a simple calculation, the maximum and minimum points are given as $(\frac{393t}{320} + \frac{23}{16}, \frac{57t}{160} - \frac{1}{8})$ and $(\frac{393t}{320} + \frac{23}{16} - \frac{7\sqrt{11}}{128}, \frac{57t}{160} - \frac{1}{8} + \frac{9\sqrt{11}}{64})$,

respectively. The maximum amplitude of the lump is approximately 2.2. As time t evolves, vibrations occur around the lump and the amplitude continues to increase. After that, a new homoclinic orbit is generated in the plane. Finally, the lump together with the new homoclinic orbit disappears into the constant background (see Fig. 4 at times $t = 5, 10$). This lump possesses the characteristic of a rogue wave in the two-dimensional physical setting, thus is referred to as the 'rogue lump'. In order to better observe the changes in the amplitude of waves in the resonant collision process, we display six curve patterns in Fig. 5 with times $t = \pm 5, \pm 4, -1, 0$ corresponding to Fig. 4. A homoclinic orbit gradually reduces its vibration frequency, as time t increases from -5 to 0. In contrast to this, another new homoclinic orbit arises from the increase of vibration frequency. When time t is large enough, the amplitude of the line wave tends to that of a plane wave. That is to say, two homoclinic orbits become plane waves, when time t tends to ∞.

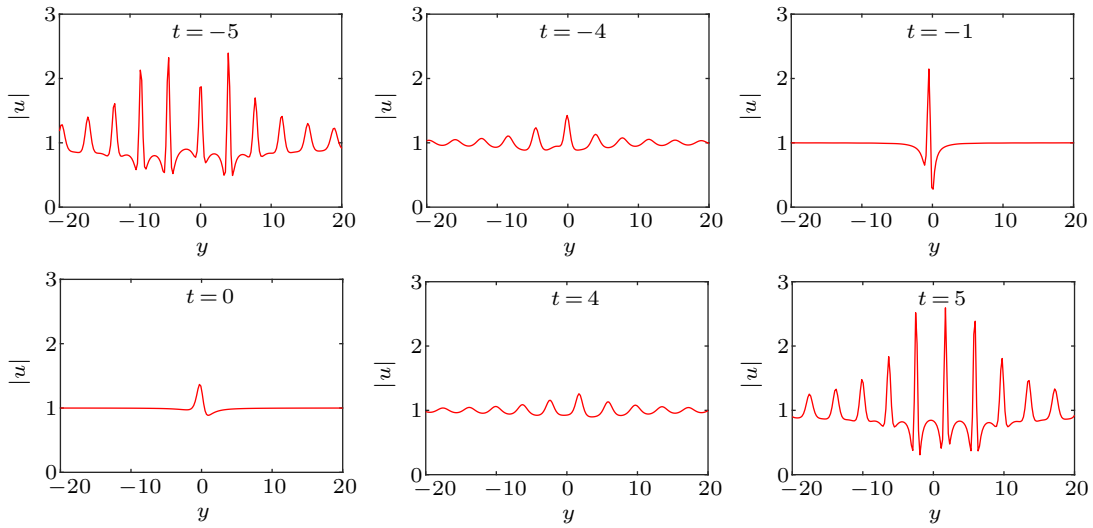


Fig. 5. The propagation curves of a rogue lump in the background of two homoclinic orbits correspond to Fig. 4.

4. High-order doubly localized waves in three-breather/homoclinic orbit backgrounds

In this section, we consider the high-order doubly rational waves moving in a three-breather or homoclinic orbit background with $K = 2$. To this end, we give the corresponding solutions as follows:

$$u(x,y,t) = \frac{g(x,y,t)}{f(x,y,t)}, \tag{15}$$

$$v(x,y,t) = 2L_1 \ln f(x,y,t), \tag{16}$$

where the functions $g(x,y,t)$, $f(x,y,t)$ are formulated as

$$g = \begin{vmatrix} m_{11}^{(1)} & m_{12}^{(1)} & m_{13}^{(1)} \\ m_{21}^{(1)} & m_{22}^{(1)} & m_{23}^{(1)} \\ m_{31}^{(1)} & m_{32}^{(1)} & m_{33}^{(1)} \end{vmatrix},$$

$$f = \begin{vmatrix} m_{11}^{(0)} & m_{12}^{(0)} & m_{13}^{(0)} \\ m_{21}^{(0)} & m_{22}^{(0)} & m_{23}^{(0)} \\ m_{31}^{(0)} & m_{32}^{(0)} & m_{33}^{(0)} \end{vmatrix}. \tag{17}$$

This solution involves three phase parameters $\xi_{i1}^{(0)}, (i = 1,2,3)$, which have a direct effect on the appearance and disappearance of line rogue waves in a breather or homoclinic orbit background.

If we let $p_{kI} = 0$, the semi-rational solutions (15)–(17) show the interaction between line rogue waves and three breathers. Taking u as an example, we set $p_1 = 1, p_2 = \frac{1}{5} - \frac{1}{2}\mathrm{i}$ in solution (15). According to the analysis in Section 2, the solution comprises at most two line-segment rogue waves and two dark rogue lumps between three breathers. In order to better understand these evolution processes, one exhibits three sets of time evolution of complete resonant collision under the phase relations $\xi_{11}^{(0)} > \xi_{21}^{(0)} > \xi_{31}^{(0)}$, $\xi_{21}^{(0)} > \xi_{11}^{(0)} > \xi_{31}^{(0)}$, and $\xi_{11}^{(0)} > \xi_{31}^{(0)} > \xi_{21}^{(0)}$ satisfying $\xi_{11}^{(0)}\xi_{31}^{(0)} < 0$. As shown in Fig. 6, the first line shows an X-shaped multi-rogue wave emerging from and merging into the three y-paralleling breather background for a short period of time. This kind of multi-rogue wave with finite length is similar to the patterns presented in the work about two line-segment rogue waves interacting with three dark line solitons for the Davey–Stewartson I equation.[65] The difference is that the line-segment rogue waves are constructed in a breather background. In addition, the line-segment rogue wave is also different from the work of Ohta,[14] where the intersection of multi-rogue waves with infinite length can attain higher amplitude at time $t = -1$ as well as lower amplitude surrounding a line wave (see the pattern in Fig. 2 in Ref. [14]). Subsequently, a completely opposite phenomenon occurs at time $t = 0$. They reach their maximum peaks at time $t = 0$, and then decay into the background of three breathers. When we choose $\xi_{21}^{(0)} = -\xi_{31}^{(0)} = 3\pi, \xi_{11}^{(0)} = 0$ in the semi-rational solutions, we show the mixed-type line

rogue wave comprising a half of a multi-line rogue wave and a line-segment rogue wave (see times $t=-0.5,0$ in Fig. 6). The multi-line rogue wave is located between the right two breathers, which is the right half of the multi-line rogue wave in the first line. The left line-segment rogue wave is an x-paralleling line wave. If we let $\xi_{11}^{(0)}=-\xi_{21}^{(0)}=3\pi,\xi_{31}^{(0)}=-2\pi$ in solution (15), there is also a mixed-type rogue wave, which evolves into a parabola-shaped rogue wave (see times $t=-1$, 0, and 1 in Fig. 4 in Ref. [14]) and a line-segment rogue wave. The parabola-shaped rogue wave originates from a lump. This mixed-type rogue wave is different from the wave displayed in the second line of Fig. 6 and has a similar wave curve to the high-order rational rogue wave solution except for a finite length (see Fig. 4 in Ref. [14]), thus is referred to as the high-order line-segment rogue wave.

If we let $p_{kl}\neq 0$, the semi-rational solutions (15)–(17) show the interaction between the second-order lumps and three breathers. The phase parameters $\xi_{i1}^{(0)}$, $(i=1,2,3)$ can be chosen as different values. For instance, when the phase parameter relation is chosen as: $\xi_{11}^{(0)}=-\xi_{31}^{(0)}=3\pi,\xi_{21}^{(0)}=0$, two rogue lumps $\mathrm{A}_1,\mathrm{A}_2$ appear from the leftmost breather then gradually move to the intermediate breather wave for a short time (see time $t=-5$, -3, 0 in Fig. 7). These two rogue lumps $\mathrm{A}_1,\mathrm{A}_2$ fuse into the intermediate breather at time $t=0$. As time t evolves, two new rogue lumps as well as an old rogue lump appear from the intermediate breather (see time $t=-3,-5$). Two new rogue lumps $\mathrm{A}_3,\mathrm{A}_4$ move towards the rightmost breather until absorbed by the latter, while the rogue lump A_2 disappears into the intermediate breather. In the whole process, there exist two complete resonant collisions between two rogue lumps and two breathers, which are different from the complete resonant interaction (see Fig. 10 in Ref. [66]). Figure 10 displays a complete resonant collision between the two rogue lumps and the bottom and top breathers, that is to say, the interaction of two rogue lumps and the intermediate breather is an elastic collision. A similar phenomenon can be seen from the complete resonant collision between two rogue lumps and three dark line solitons (see Fig. 5 in Ref. [65]). When the phase parameter relation is chosen as: $\xi_{11}^{(0)}=-\xi_{31}^{(0)}=3\pi,\xi_{21}^{(0)}=-2\pi$ in solutions (15), there exist a second-order rogue lump and a dark rogue lump in the background of three breathers. As shown in Fig. 8, the second-order rogue lump comprising two rogue lumps $\mathrm{A}_1,\mathrm{A}_2$ appears from the leftmost breather and happens to gather before coming into contact with the intermediate breather. After that, the rogue lump A_1 fuses into the intermediate breather and the rogue lump A_2 passes through it, meanwhile a new dark rogue lump B appears from the latter and moves to the rightmost breather. Finally, all these rogue lumps disappear into the rightmost breather. In the stage of input and output, there is no rogue lump. Furthermore, there exist other complete resonant collisions between the second-order rogue lump and three breathers, when the phase parameter relations are chosen as other types.

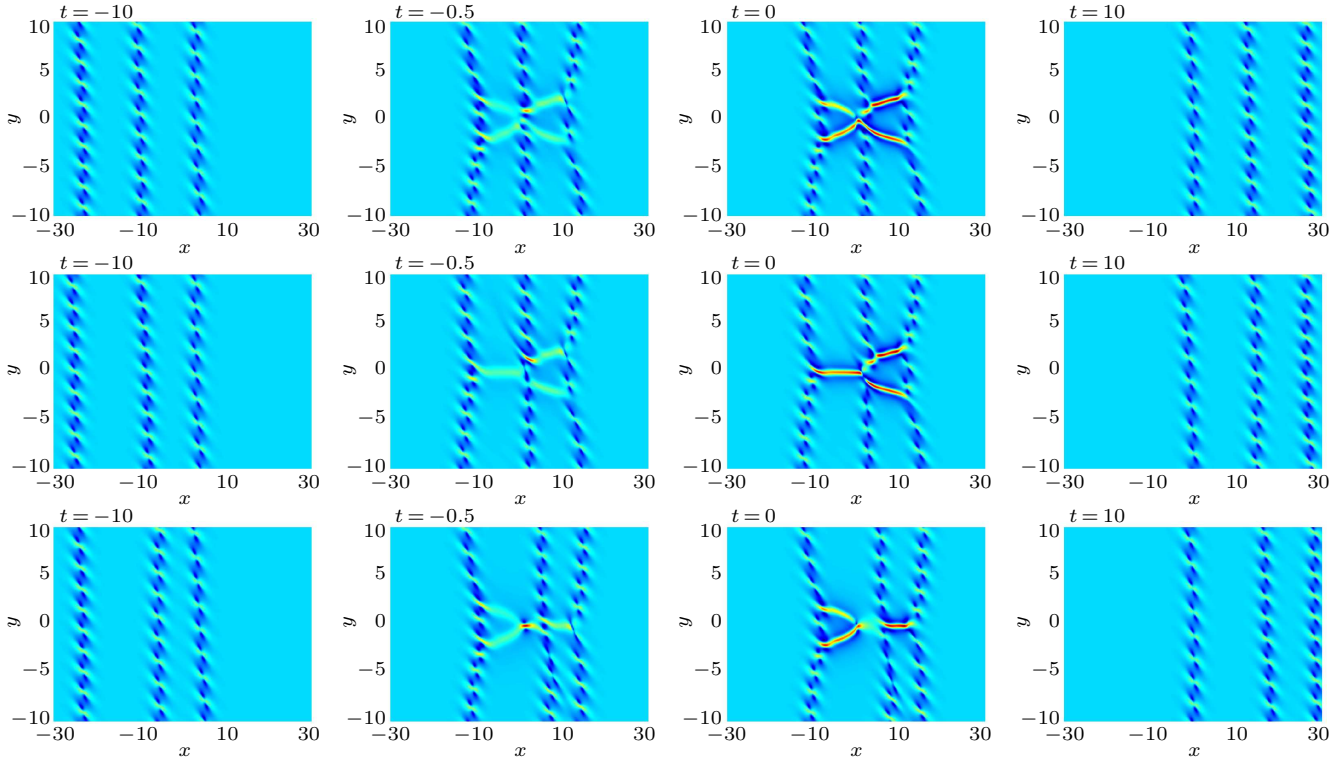


Fig. 6. The time evolution of multi-rogue wave, mixed-type wave of multi-rogue wave and line-segment rogue wave, and high-order rogue wave of parabola-shaped rogue waves and line-segment rogue wave in a three-breather background via parameters: $p_1=1$, $p_2=\frac{1}{5}-\frac{1}{2}\mathrm{i}$, the first line: $\xi_{11}^{(0)}=-\xi_{21}^{(0)}=3\pi$, $\xi_{31}^{(0)}=0$, the second line: $\xi_{21}^{(0)}=-\xi_{31}^{(0)}=3\pi$, $\xi_{11}^{(0)}=0$, the third line: $\xi_{11}^{(0)}=-\xi_{21}^{(0)}=3\pi$, $\xi_{31}^{(0)}=-2\pi$.

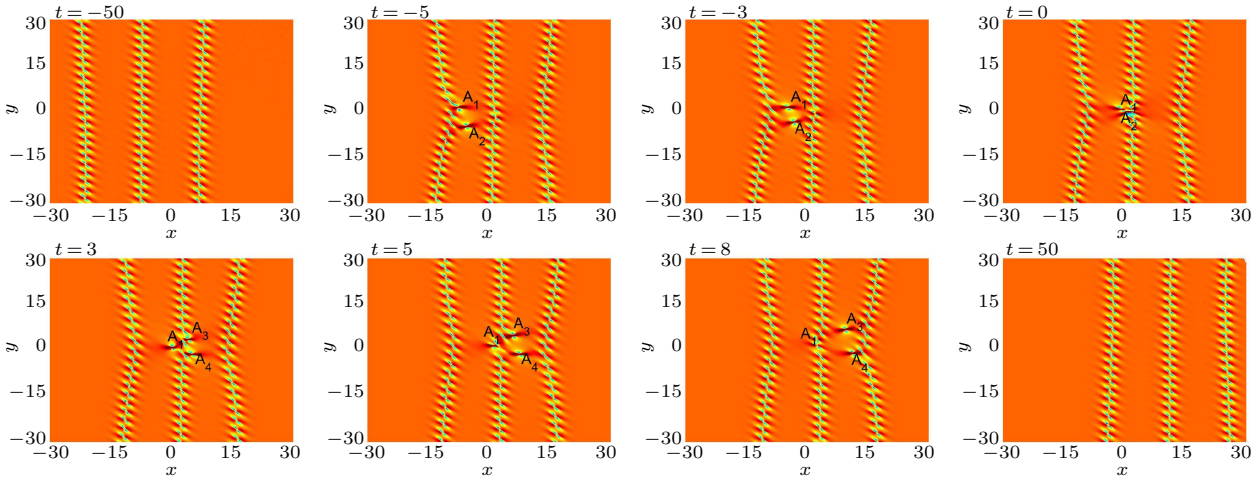


Fig. 7. The time evolution of high-order rogue lumps in a three-breather background via parameters: $p_1 = 1 - \frac{1}{2}\mathrm{i}$, $p_2 = \frac{7}{50} - \frac{1}{2}\mathrm{i}$, $\xi_{11}^{(0)} = -\xi_{31}^{(0)} = 3\pi$, $\xi_{21}^{(0)} = 0$.

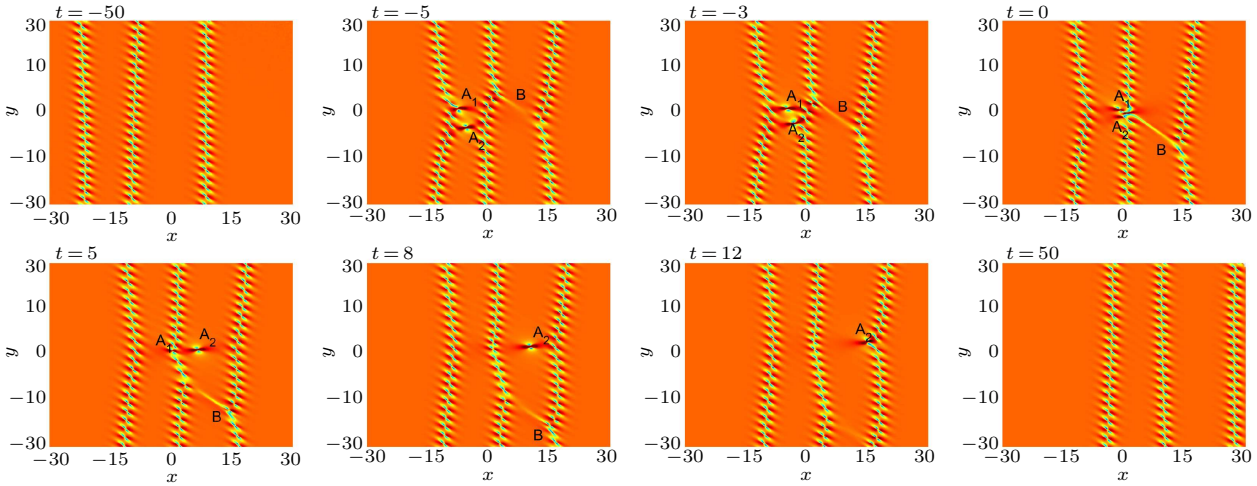


Fig. 8. The time evolution of high-order rogue lumps in a three-breather background via parameters: $p_1 = 1 - \frac{1}{2}\mathrm{i}$, $p_2 = \frac{7}{50} - \frac{1}{2}\mathrm{i}$, $\xi_{11}^{(0)} = -\xi_{21}^{(0)} = 3\pi$, $\xi_{31}^{(0)} = 0$.

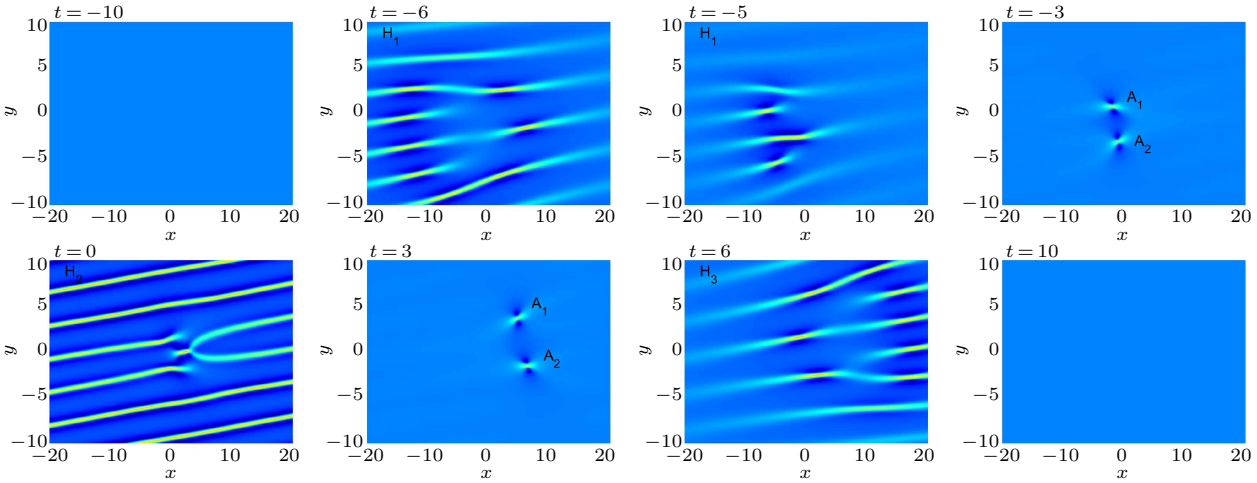


Fig. 9. The time evolution of high-order rogue lumps in a homoclinic orbit background via parameters: $p_1 = p_2^* = 1 - \frac{1}{2}\mathrm{i}$, $\xi_{11}^{(0)} = -\xi_{31}^{(0)} = 2\pi$, $\xi_{21}^{(0)} = 0$.

Next, we choose the parameter values $p_1 = p_2^* = 1 - \frac{1}{2}\mathrm{i}$ in the semi-rational solutions (15). The multi-breathers transform into the homoclinic orbits under the choice of this kind of phase parameters. That is to say, the semi-rational solutions show the interaction of doubly localized lumps with multiple homoclinic orbits. As shown in Fig. 9, when the phase parameter relation is chosen as: $\xi_{11}^{(0)} = -\xi_{31}^{(0)} = 2\pi, \xi_{21}^{(0)} = 0$, only a second-order doubly localized lump comprising two rogue lumps A_1 and A_2 emerges and disappears amidst three homoclinic orbits $\mathrm{H}_i, i = 1, 2, 3$. We observe that a homoclinic orbit H_1 first emerges from the constant background. Then,

the homoclinic orbit H_1 reduces its amplitude and intensity, and generates a protrusion in a local area. At time $t=-3$, the protrusion excites two rogue lumps A_1 and A_2. Later, the homoclinic orbit H_1 disappears from the constant background for a very short time. As time t evolves, the homoclinic orbit H_2 appears and attains its highest amplitude at time $t=0$, then quickly decays into the constant background. Meanwhile, two rogue lumps keep moving forward. Finally, the homoclinic orbit H_3 emerges, and two rogue lumps merge into it and subsequently vanish together with it into the background (see time $t=6,10$). During this time evolution process, two rogue lumps and three homoclinic orbits exist for a very short time. As shown in Fig. 10, when the phase parameter relation is chosen as: $\xi_{11}^{(0)}=-\xi_{21}^{(0)}=2\pi, \xi_{31}^{(0)}=0$, the homoclinic orbit H_1 first appears from the constant background. Then a rogue lump A_1 moves along the positive x-direction, and a rogue lump $A_2^{(1)}$ moves along the negative x-direction. Another rogue lump $A_2^{(2)}$ appears from the background, following the rogue lump A_1, and together with the homoclinic orbit H_2 disappears from the constant background. Then two rogue lumps $A_2^{(1)}, A_2^{(2)}$ exist in the background. Finally, the two rogue lumps are absorbed by the homoclinic orbit H_3, and together with it decay into the constant background.

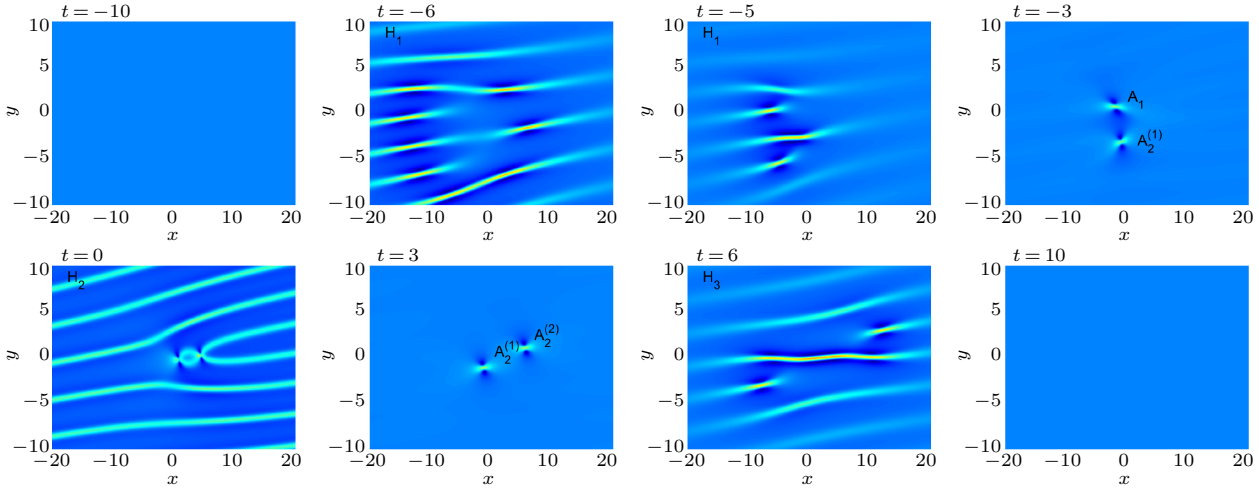


Fig. 10. The time evolution of high-order rogue lumps in a homoclinic orbit background via parameters: $p_1=p_2^*=1-\frac{1}{2}\mathrm{i}$, $\xi_{11}^{(0)}=-\xi_{21}^{(0)}=2\pi$, $\xi_{31}^{(0)}=0$.

5. Conclusion

This paper systematically investigates the (2+1)-dimensional Maccari system using Hirota's bilinear method and the KP hierarchy reduction method. We build upon the results in Ref. [60], which only focused on partial resonant collisions between rational waves and one breather. We analyze the doubly localized behaviors of rogue lumps or line-segment rogue waves in multi-breather and homoclinic orbit backgrounds. Specifically, we examine a second-order complete resonant solution comprising two rational waves with a phase difference, which do not occur simultaneously, and two breathers or homoclinic orbits. In a two-breather background, we observe a rogue lump emerging from one breather and disappearing into the other breather momentarily. However, in a homoclinic orbit background, we observe a different phenomenon where the rogue lump appears, followed by the first homoclinic orbit, and maintains its state for a period of time before the second homoclinic orbit appears. Eventually, the rogue lump, together with the second homoclinic orbit, decays to the constant background. Furthermore, the third-order doubly localized wave solution demonstrates the presence of high-order rational waves in three breathers and homoclinic orbit backgrounds, which becomes more complex due to the inclusion of three phase parameters. In addition to the theoretical findings presented in this work, the potential experimental realization of the doubly localized waves, such as rogue lumps and line-segment rogue waves, can be performed. These structures may be experimentally observable in physical systems described by the (2+1)-dimensional nonlinear system.

Acknowledgements

The authors would like to thank the Editor and Reviewers for their valuable comments. Project supported by the Natural Science Research Start-up Foundation of Recruiting Talents of Nanjing University of Posts and Telecommunications (Grant Nos. NY225085 and NY225004).

References

[1] Ablowitz M J and Clarkson P A 1991 *Solitons, Nonlinear Evolution Equations and Inverse Scattering* (Cambridge: Cambridge University Press)
[2] Pelinovsky D E, Stepanyants Y A and Kivshar Y S 1995 *Phys. Rev. E* **51** 5016
[3] Infeld E and Rowlands G 2000 *Nonlinear Waves, Solitons and Chaos* (Cambridge: Cambridge University Press)
[4] Mironov V A, Smirnov A I and Smirnov L A 2010 *JETP* **110** 877
[5] Abramyan L A and Stepanyants Y A 1985 *Sov. Phys. JETP* **61** 963
[6] Draper L 1966 *Weather* **21** 2

[7] Akhmediev N, Ankiewicz A and Taki M 2009 *Phys. Lett. A* **373** 675
[8] Moslem W M, Shukla P K and Eliasson B 2011 *Eur. Phys. Lett.* **96** 25002
[9] Xu S W and He J S 2012 *J. Math. Phys.* **53** 063507
[10] Solli D R, Ropers C, Koonath P and Jalali B 2007 *Nature* **450** 1054
[11] Bludov Y V, Konotop V V and Akhmediev N 2010 *Eur. Phys. J: Spec. Top.* **185** 169
[12] Stenflo L and Marklund M 2010 *Plasma Phys.* **76** 293
[13] Yan Z 2011 *Phys. Lett. A* **375** 4274
[14] Ohta Y and Yang J 2012 *Phys. Rev. E* **86** 036604
[15] Ohta Y and Yang J 2013 *J. Phys. A* **46** 105202
[16] Akhmediev N, Ankiewicz A and Taki M 2009 *Phys. Lett. A* **373** 675
[17] Kuznetsov E 1977 *Sov. Phys. Dokl.* **22** 507
[18] Ma Y C 1979 *Stud. Appl. Math.* **60** 43
[19] Tajiri M and Watanabe Y 1998 *Phys. Rev. E* **57** 3510
[20] Xu G, Gelash A, Chabchoub A, Zakharov V and Kibler B 2019 *Phys. Rev. Lett.* **122** 084101
[21] Wang M, Xu T and He G 2023 *Chin. Phys. B* **32** 050503
[22] Kibler B, Chabchoub A, Gelash A, Akhmediev N and Zakharov V E 2013 *Phys. Rev. X* **5** 041026
[23] Liu C, Ren Y, Yang Z Y and Yang W L 2017 *Chaos* **27** 083120
[24] Matveev V B and Salle M A 1991 *Darboux transformations and solitons* (Berlin: Springer)
[25] Wang X and Chen Y 2014 *Chin. Phys. B* **23** 070203
[26] Du Z, Tian B and Qu Q X 2020 *Chin. Phys. B* **29** 030202
[27] Xu T, Chen Y and Lin J 2017 *Chin. Phys. B* **26** 120201
[28] Tao Y S, He J S and Porsezian K 2013 *Chin. Phys. B* **22** 074210
[29] Ablowitz M J and Segur H 1981*Solitons and Inverse Scattering Transform* (Philadelphia: SIAM)
[30] Wen L, Zhang N and Fan E 2020 *Acta Math. Sci.* **40** 113
[31] Wen L, Fan E and Chen Y 2023 *Acta Math. Sci.* **43** 1045
[32] Hirota R 1980 *Direct Methods in Soliton Theory* (Berlin: Springer)
[33] Yang B and Yang J 2021 *IMA J. Appl. Math.* **86** 378
[34] Feng B F, Shi C, Zhang G and Wu C 2022 *J. Phys. A* **55** 235701
[35] Han Z, Chen Y and Chen J C 2017 *J. Phys. Soc. Jpn.* **86** 104008
[36] Feng B F 2014 *J. Phys. A* **47** 355203
[37] Chen J, Chen Y, Feng B F and Maruno K 2015 *Phys. Lett. A* **379** 1510
[38] Wang X B and Tian S F 2022 *Physica D* **442** 133528
[39] Tian S F 2017 *J. Differ. Equ.* **262** 506
[40] Li Z Q, Tian S F and Yang J J 2022 *Adv. Math.* **409** 108639
[41] Mao J J, Xu T Z and Shi L F 2023 *Z. Angew. Math. Phys.* **74** 78
[42] Yan X W and Chen Y 2025 *Annal. Phys.* **478** 170000
[43] Yan X W, Tian S F, Dong M J and Zhang T T 2019 *J. Phys. Soc. Jpn.* **88** 074004
[44] Rao J, Cheng Y and He J 2017 *Stud. Appl. Math.* **139** 568
[45] Rao J, Zhang Y, Fokas A S and He J 2018 *Nonlinearity* **31** 4090
[46] Yang B and Yang J 2022 *Physica D* **432** 133160
[47] Cao Y, Cheng Y, Malomed B A and He J 2021 *Stud. Appl. Math.* **147** 694
[48] Miles J W 1977 *J. Fluid Mech.* **79** 157
[49] Miles J W 1977 *J. Fluid Mech.* **79** 171
[50] Rao J, Chow K W, Mihalache D and He J 2021 *Stud. Appl. Math.* **147** 1007
[51] Chen J, Yang B and Feng B F 2023 *Stud. Appl. Math.* **151** 1020
[52] Zhao N, Chen Y, Cheng L and Chen J 2025 *Nonlinear Dyn.* **113** 8801
[53] Wang D, Liu Z, Zhao H and Dai C 2025 *Science* **389** 935
[54] Rao J, Kanna T, Mihalache D and He J 2022 *Physica D* **439** 133281
[55] Ma W X and Zhou Y 2018 *J. Differ. Equ.* **264** 2633
[56] Ma W X 2015 *Phys. Lett. A* **379** 1975
[57] Maccari A 1996 *J. Math. Phys.* **37** 6207
[58] Maccari A 2020 *Phys. Lett. A* **384** 126740
[59] Jiang Y, Rao J, Mihalache D, He J and Cheng Y 2021 *Commun. Nonlinear Sci. Numer. Simul.* **102** 105943
[60] Cao Y, Cheng Y and He J 2023 *J. Math. Phys.* **64** 043501
[61] Han Z and Chen Y 2017 *Chin. Phys. Lett.* **34** 070202
[62] Ma H, Qi X, Deng A 2023 *Chin. Phys. B* **32** 120503
[63] Meng Y, Fang P P, Lin J 2024 *Chin. Phys. Lett.* **41** 060501
[64] Ohta Y and Yang J 2012 *Proc. Roy. Soc. A* **468** 1716
[65] Rao J, Fokas A S and He J 2021 *J. Nonlinear Sci.* **31** 67
[66] Rao J, Kanna T and He J 2022 *Proc. Roy. Soc. A* **478** 20210777